Perfect narrow band absorber for sensing applications

Shiwen Luo, Jun Zhao, Duluo Zuo,* and Xinbing Wang

Wuhan National Laboratory for Optoelectronics, Huazhong University of Science and Technology, Wuhan 430074, China

*zuoduluo@hust.edu.cn

Abstract: We design and numerically investigate a perfect narrow band absorber based on a metal-metal-dielectric-metal structure which consists of periodic metallic nanoribbon arrays. The absorber presents an ultra narrow absorption band of 1.11 nm with a nearly perfect absorption of over 99.9% in the infrared region. For oblique incidence, the absorber shows an absorption more than 95% for a wide range of incident angles from 0 to 50°. Structure parameters to the influence of the performance are investigated. The structure shows high sensing performance with a high sensitivity of 1170 nm/RIU and a large figure of merit of 1054. The proposed structure has great potential as a biosensor.

OCIS codes: (240.6680) Surface plasmons; (280.4788) Optical sensing and sensors; (310.6628) Subwavelength structures, nanostructures.

References and links

1. W. L. Barnes, A. Dereux, and T. W. Ebbesen, "Surface plasmon subwavelength optics," Nature **424**(6950), 824–830 (2003).
2. J. M. Pitarke, V. M. Silkin, E. V. Chulkov, and P. M. Echenique, "Theory of surface plasmons and surface-plasmon polaritons," Rep. Prog. Phys. **70**(1), 1–87 (2007).
3. D. K. Gramotnev and S. I. Bozhevolnyi, "Plasmonics beyond the diffraction limit," Nat. Photonics **4**(2), 83–91 (2010).
4. A. G. Brolo, "Plasmonics for future biosensors," Nat. Photonics **6**(11), 709–713 (2012).
5. I. Park, S. Kim, J. Choi, D. Lee, Y. Kim, M. F. Kling, M. I. Stockman, and S. Kim, "Plasmonic generation of ultrashort extreme-ultraviolet light pulses," Nat. Photonics **5**(11), 677–681 (2011).
6. S. Zhang, H. Wei, K. Bao, U. Håkanson, N. J. Halas, P. Nordlander, and H. Xu, "Chiral surface plasmon polaritons on metallic nanowires," Phys. Rev. Lett. **107**(9), 096801 (2011).
7. Y. Zhang, J. Wang, J. Shen, Z. Man, W. Shi, C. Min, G. Yuan, S. Zhu, H. P. Urbach, and X. Yuan, "Plasmonic hybridization induced trapping and manipulation of a single Au nanowire on a metallic surface," Nano Lett. **14**(11), 6430–6436 (2014).
8. M. Yang, R. Alvarez-Puebla, H. S. Kim, P. Aldeanueva-Potel, L. M. Liz-Marzán, and N. A. Kotov, "SERS-active gold lace nanoshells with built-in hotspots," Nano Lett. **10**(10), 4013–4019 (2010).
9. Y. Wang, T. Sun, T. Paudel, Y. Zhang, Z. Ren, and K. Kempa, "Metamaterial-plasmonic absorber structure for high efficiency amorphous silicon solar cells," Nano Lett. **12**(1), 440–445 (2012).
10. C. F. Guo, T. Sun, F. Cao, Q. Liu, and Z. Ren, "Metallic nanostructures for light trapping in energy-harvesting devices," Light Sci. Appl. **3**(4), e161 (2014).
11. X. Liu, T. Tyler, T. Starr, A. F. Starr, N. M. Jokerst, and W. J. Padilla, "Taming the blackbody with infrared metamaterials as selective thermal emitters," Phys. Rev. Lett. **107**(4), 045901 (2011).
12. C. Argyropoulos, K. Q. Le, N. Mattiucci, G. D. Aguanno, and A. Alu, "Broadband absorbers and selective emitters based on plasmonic Brewster metasurfaces," Phys. Rev. B **87**(20), 205112 (2013).
13. Y. Li, L. Su, C. Shou, C. Yu, J. Deng, and Y. Fang, "Surface-enhanced molecular spectroscopy (SEMS) based on perfect-absorber metamaterials in the mid-infrared," Sci. Rep. **3**, 2865 (2013).
14. A. A. Jamali and B. Witzigmann, "Plasmonic perfect absorbers for biosensing applications," Plasmonics **9**(6), 1265–1270 (2014).
15. N. I. Landy, S. Sajuyigbe, J. J. Mock, D. R. Smith, and W. J. Padilla, "Perfect metamaterial absorber," Phys. Rev. Lett. **100**(20), 207402 (2008).
16. Z. Fang, Y. Zhen, L. Fan, X. Zhu, and P. Nordlander, "Tunable wide-angle plasmonic perfect absorber at visible frequencies," Phys. Rev. B **85**(24), 245401 (2012).
17. M. K. Hedayati, M. Javaherirahim, B. Mozooni, R. Abdelaziz, A. Tavassolizadeh, V. S. K. Chakravadhanula, V. Zaporojtchenko, T. Strunkus, F. Faupel, and M. Elbahri, "Design of a perfect black absorber at visible frequencies using plasmonic metamaterials," Adv. Mater. **23**(45), 5410–5414 (2011).
18. X. Shen, Y. Yang, Y. Zang, J. Gu, J. Han, W. Zhang, and T. J. Cui, "Triple-band terahertz metamaterial

#256039 Received 22 Dec 2015; revised 23 Mar 2016; accepted 18 Apr 2016; published 20 Apr 2016

absorber: Design, experiment, and physical interpretation," Appl. Phys. Lett. **101**(15), 154102 (2012).
19. M. G. Nielsen, A. Pors, O. Albrektsen, and S. I. Bozhevolnyi, "Efficient absorption of visible radiation by gap plasmon resonators," Opt. Express **20**(12), 13311–13319 (2012).
20. H. Tao, C. M. Bingham, A. C. Strikwerda, D. Pilon, D. Shrekenhamer, N. I. Landy, K. Fan, X. Zhang, W. J. Padilla, and R. D. Averitt, "Highly flexible wide angle of incidence terahertz metamaterial absorber: design, fabrication, and characterization," Phys. Rev. B **78**(24), 241103 (2008).
21. N. Liu, M. Mesch, T. Weiss, M. Hentschel, and H. Giessen, "Infrared perfect absorber and its application as plasmonic sensor," Nano Lett. **10**(7), 2342–2348 (2010).
22. M. K. Hedayati, M. Javaherirahim, B. Mozooni, R. Abdelaziz, A. Tavassolizadeh, V. S. K. Chakravadhanula, V. Zaporojtchenko, T. Strunkus, F. Faupel, and M. Elbahri, "Design of a perfect black absorber at visible frequencies using plasmonic metamaterials," Adv. Mater. **23**(45), 5410–5414 (2011).
23. Y. Cui, K. H. Fung, J. Xu, H. Ma, Y. Jin, S. He, and N. X. Fang, "Ultrabroadband light absorption by a sawtooth anisotropic metamaterial slab," Nano Lett. **12**(3), 1443–1447 (2012).
24. Y. Cui, J. Xu, K. H. Fung, Y. Jin, A. Kumar, S. He, and N. X. Fang, "A thin film broadband absorber based on multi-sized nanoantennas," Appl. Phys. Lett. **99**(25), 253101 (2011).
25. L. Huang, D. R. Chowdhury, S. Ramani, M. T. Reiten, S. N. Luo, A. J. Taylor, and H. T. Chen, "Experimental demonstration of terahertz metamaterial absorbers with a broad and flat high absorption band," Opt. Lett. **37**(2), 154–156 (2012).
26. K. Aydin, V. E. Ferry, R. M. Briggs, and H. A. Atwater, "Broadband polarization-independent resonant light absorption using ultrathin plasmonic super absorbers," Nat. Commun. **2**, 517 (2011).
27. Z. Liu, G. Liu, X. Liu, S. Huang, Y. Wang, P. Pan, and M. Liu, "Achieving an ultra-narrow multiband light absorption meta-surface via coupling with an optical cavity," Nanotechnology **26**(23), 235702 (2015).
28. L. J. Sherry, S. H. Chang, G. C. Schatz, R. P. Van Duyne, B. J. Wiley, and Y. Xia, "Localized surface plasmon resonance spectroscopy of single silver nanocubes," Nano Lett. **5**(10), 2034–2038 (2005).
29. F. Hao, P. Nordlander, Y. Sonnefraud, P. Van Dorpe, and S. A. Maier, "Tunability of subradiant dipolar and fano-type plasmon resonances in metallic ring/disk cavities: implications for nanoscale optical sensing," ACS Nano **3**(3), 643–652 (2009).
30. Y. B. Zheng, Y. W. Yang, L. Jensen, L. Fang, B. K. Juluri, A. H. Flood, P. S. Weiss, J. F. Stoddart, and T. J. Huang, "Active molecular plasmonics: controlling plasmon resonances with molecular switches," Nano Lett. **9**(2), 819–825 (2009).
31. A. V. Kabashin, P. Evans, S. Pastkovsky, W. Hendren, G. A. Wurtz, R. Atkinson, R. Pollard, V. A. Podolskiy, and A. V. Zayats, "Plasmonic nanorod metamaterials for biosensing," Nat. Mater. **8**(11), 867–871 (2009).
32. Y. Shen, J. Zhou, T. Liu, Y. Tao, R. Jiang, M. Liu, G. Xiao, J. Zhu, Z. K. Zhou, X. Wang, C. Jin, and J. Wang, "Plasmonic gold mushroom arrays with refractive index sensing figures of merit approaching the theoretical limit," Nat. Commun. **4**, 2381 (2013).
33. Z. Liu, H. Shao, G. Liu, X. Liu, H. Zhou, Y. Hu, X. Zhang, Z. Cai, and G. Gu, "λ3/20000 plasmonic nanocavities with multispectral ultra-narrowband absorption for high-quality sensing," Appl. Phys. Lett. **104**(8), 081116 (2014).
34. X. Lu, L. Zhang, and T. Zhang, "Nanoslit-microcavity-based narrow band absorber for sensing applications," Opt. Express **23**(16), 20715–20720 (2015).
35. M. A. Ordal, L. L. Long, R. J. Bell, S. E. Bell, R. R. Bell, R. W. Alexander, Jr., and C. A. Ward, "Optical properties of the metals Al, Co, Cu, Au, Fe, Pb, Ni, Pd, Pt, Ag, Ti, and W in the infrared and far infrared," Appl. Opt. **22**(7), 1099–1119 (1983).
36. E. D. Palik, *Handbook of Optical Constants of Solids* (Academic Press, 1998).

1. Introduction

Surface plasmon polaritons(SPPs) are surface electromagnetic wave propagating along a metal-dielectric interface and have great potential applications in the realization of highly integrated optical circuits due to their capability to overcome the diffraction limit of light [1, 2]. In recent years, extraordinary optical properties in metallic nanostructures have attracted much attention due to their promising applications [3–8]. However, the intrinsic losses are inevitable in these structures which often limit their performance. For a metamaterial absorber, however, the intrinsic losses can be enhanced remarkly and achieve perfect absorption by proper design of the resonance structure. Perfect metamaterial absorbers have been rapidly developed due to their applications such as energy harvesting [9, 10], thermal emitting [11, 12], and biosensing [13, 14]. The first perfect metamaterial absorber was demonstrated by Landy *et al*. Since then many different kinds of perfect absorbers have been proposed from terahertz region to visible region [15–19]. Tao *et al* presented a terahertz absorber based on an array of 200-nm-thick Au electrically resonant split ring resonators which operated over a wide range of angles of incidence for both transverse electric and transverse magnetic radiation [20]. Liu *et al* designed a gold disk array structure and presented the absorption of 99% in the infrared region [21]. Hedayati *et al* designed a perfect

#256039 Received 22 Dec 2015; revised 23 Mar 2016; accepted 18 Apr 2016; published 20 Apr 2016

absorber in the visible region by a combination of a metal film with suitable metal/dielectric nanocomposites [22].

In practical applications perfect absorbers can be generally categorized into broadband absorbers and narrowband absorbers in terms of their absorption bandwidths [23–27]. For a biosensor, narrower band will improve the performance. In sensing applications, bulk sensitivity (S) and figure of merit (FOM) are usually used to evaluate the sensing performance. S and FOM are defined as $S = \Delta\lambda/\Delta n$, FOM = S/FWHM respectively, where Δn is the refractive index change, $\Delta\lambda$ is the resonance wavelength change owing to the refractive index change, FWHM is the full width at half maximum of the spectrum [28]. In order to improve the sensing performance, many structures have been designed including nanorings [29], nanodisks [21, 30], nanorods [31], and so on. Shen *et al* designed a gold mushroom arrays structure with a narrow FWHM of 10 nm and a high FOM of 108 [32]. Liu *et al* designed a cross-shape patch array structure with FWHM of 12 nm and S of 538 nm/RIU (refractive index unit) [33]. Lu *et al* proposed a nanoslit microcavity based structure and demonstrated a narrower FWHM of 8 nm [34].

In this work, we demonstrate a perfect narrow band absorber based on a metal-metal-dielectric-metal (MMDM) structure working at the infrared region. In this structure, a nearly perfect absorption of over 99.9% is realized with FWHM of only 1.11 nm. The structure can keep absorption performance over a wide range of incident angle. We investigate the influence of the structure parameters on the optical properties and check the properties of the structure as a sensor. The proposed structure can be used in biomedical applications.

2. Structure and numerical simulations

2.1 Structure

The schematic geometry of the proposed MMDM structure is shown in Fig. 1(a). Periodic metallic nanoribbon arrays which consist of a top layer nanoribbon array and a down layer nanoribbon array are deposited on a SiO_2 dielectric layer supported by a metallic film. Figure 1(b) shows the cross section of the MMDM structure. The structure has dimensional parameters as follows: top layer nanoribbon width w_1, w_2, down layer nanoribbon width d which is also the distance between two top layer nanoribbons, top layer nanoribbon thickness t_1, down layer nanoribbon thickness t_2, dielectric layer thickness h and structure period P. Here, we choose gold as the material of the metallic nanoribbon array and the permittivity of gold is taken from [35]. The refractive index of the dielectric layer SiO_2 is taken from [36]. To compare with the MMDM structure, the metallic grating structure without the SiO_2 dielectric layer shown in Fig. 1(c) is also investigated.

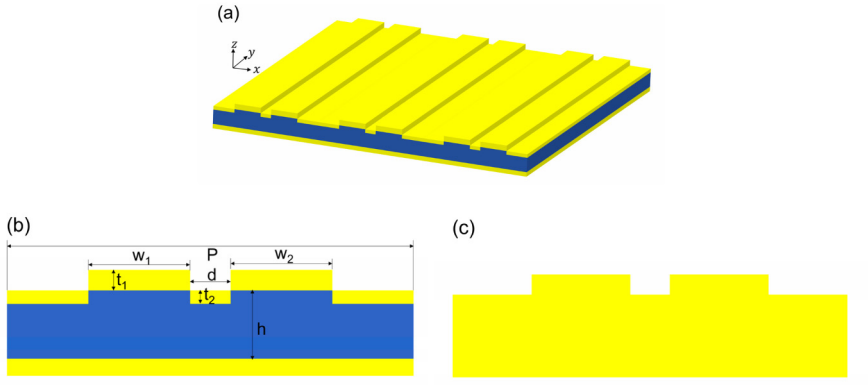

Fig. 1. (a) Schematic of the MMDM structure. (b) Cross-section of the MMDM structure of an unit cell. (c) Cross-section of the corresponding metallic grating structure without the dielectric layer.

#256039 Received 22 Dec 2015; revised 23 Mar 2016; accepted 18 Apr 2016; published 20 Apr 2016

To investigate the optical properties of the designed structure, we use two-dimensional finite element methods realized in COMSOL MULTIPHYSICS for calculations. As the gold film is thicker than the penetration depth of the infrared light, the incident light will be blocked and the transmittance (T) of the structure is nearly zero ($T = 0$) and the absorption $A = 1 - R$ (reflection). A normally incident plane wave along the negative z direction polarized along the x direction is applied.

2.2 Results and discussions

Figure 2(a) shows the reflection and absorption spectra of the MMDM structure and the metallic grating structure. Geometric parameters of the structure are given as follows: $w_1 = w_2 = w = 300$ nm, $d = 80$ nm, $t_1 = 60$ nm, $t_2 = 40$ nm, $h = 200$ nm, $P = 1200$ nm. The red solid line shows a nearly perfect absorption property at the resonant wavelength of 1564.5 nm with the peak absorption over 99.9% for the MMDM structure at normal incidence. For comparison, the magenta dash line shows the peak absorption of only 70.9% for the metallic grating structure. The FWHM of the two structures are 1.11 nm and 1.54 nm respectively.

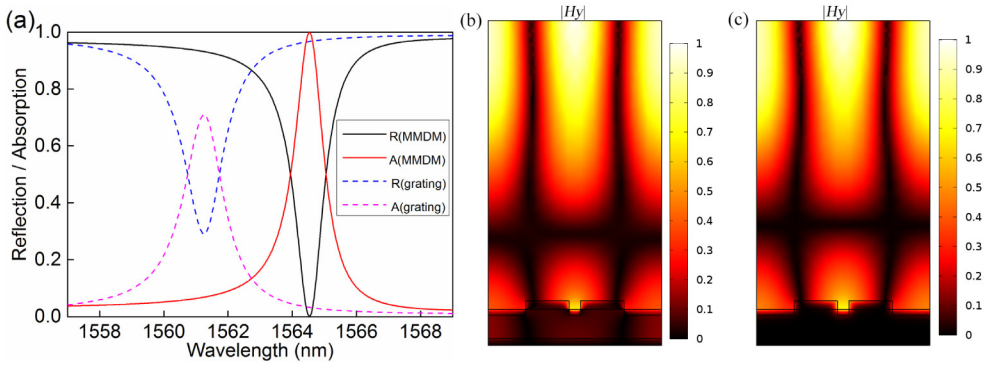

Fig. 2. (a) The absorption and reflection spectra of the corresponding metallic grating structure and the MMDM structure. (b) The magnetic field distributions at the resonant wavelength of the MMDM structure. (c). The magnetic field distributions at the resonant wavelength of the corresponding metallic grating structure. Parameters of the MMDM structure are set as $w = 300$ nm, $d = 80$ nm, $t_1 = 60$ nm, $t_2 = 40$ nm, $h = 200$ nm and $P = 1200$ nm.

In order to understand the underlying physics of the sharp absorption peak, the magnetic field distributions at the resonant wavelength of the MMDM structure and the metallic grating structure are calculated and presented in Fig. 2(b) and Fig. 2(c) respectively. Figure 2(b) shows that most magnetic field is located between the nanoribbons and some transmits into the dielectric layer which indicates that the coupling between the nanoribbons and the gold film contributes to the perfect absorption. From Fig. 2(c), the magnetic field is located on the surface and between the nanoribbons which indicates that the surface plasmons cannot pass through the metals but propagate on the surface.

In order to analyze the resonant behavior of the MMDM structure, absorption properties at oblique incidence are presented. Figure 3(a) shows that as the incident angle θ increases from 0° to 80°, the absorption decreases and the resonant wavelength keeps nearly unchanged. From Fig. 3(b), the MMDM structure is capable of absorbing 99% of the light at the resonant wavelength for the incident angles from 0 to 30°. The absorption is more than 95% for a wide range of incident angles from 0 to 50°. As shown in Figs. 3(c) and 3(d), the absorption is more sensitive to the incident angle for the corresponding metallic grating structure. The range of incident angles is about 15° for the absorption bigger than 95%.

#256039 Received 22 Dec 2015; revised 23 Mar 2016; accepted 18 Apr 2016; published 20 Apr 2016

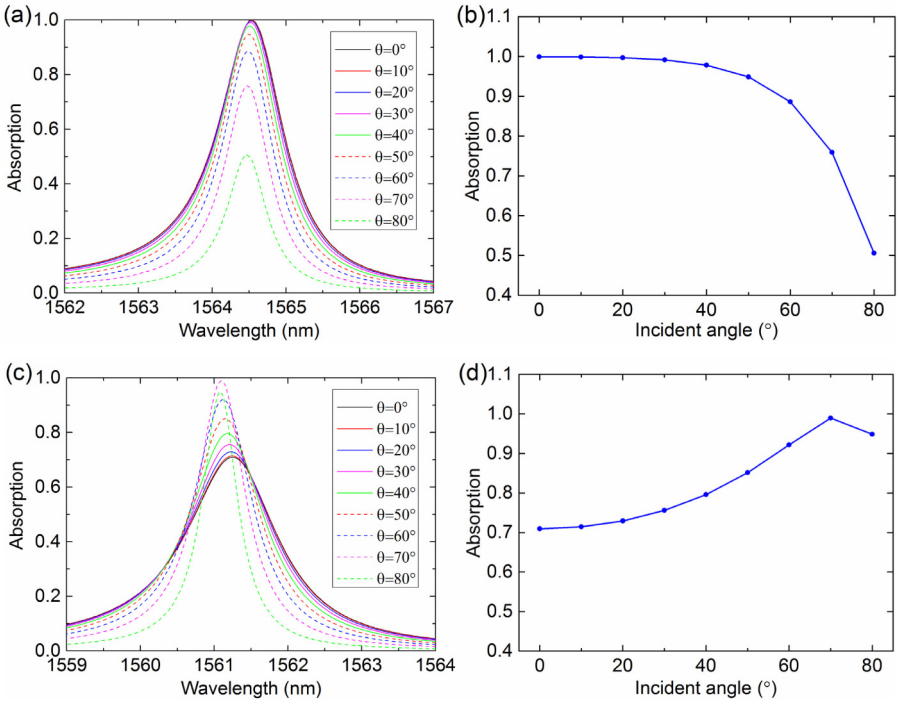

Fig. 3. (a) Absorption spectra of the MMDM structure as functions of the incident angle. (b) Peak absorption of the MMDM structure as functions of the incident angle. (c) Absorption spectra of the corresponding metallic grating structure as functions of the incident angle. (d) Peak absorption of the corresponding metallic grating structure as functions of the incident angle.

As shown in Fig. 4, the influence of structure parameters on the reflectivity of the resonance dip and the FWHM of the MMDM are investigated. According to Fig. 4(a), when the top layer nanoribbon thickness t_1 changes from 30 nm to 110 nm, FWHM become narrower and changes from 1.13 nm to 0.54 nm while the reflectivity of the resonance dip decreases first and then increases. Figure 4(b) shows decrease of FWHM and increase of the reflectivity as the distance between two top layer nanoribbons d changes from 40 nm to 180nm. Figure 4(c) shows that when the top layer nanoribbon width w incerases from 180 nm to 420 nm, FWHM decerases while the reflectivity decreases first and the increases slightly.

For a biosensor, lower reflectivity of the resonance dip and narrower FWHM of the resonance spectrum are essential. From Figs. 4(a)-(c), reflectivity and FWHM can't be optimized simultaneously. For structure design, robustness is important. In our design, when the structure parameters change, FWHM changes slightly and the reflectivity keeps low in a wide range which is beneficial to structure design.

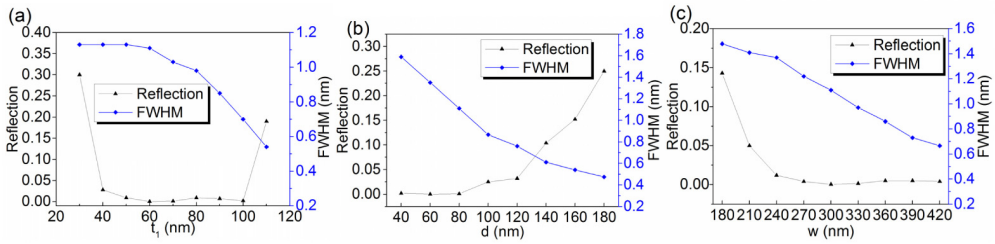

Fig. 4. (a)-(c) Reflectivity of the resonance dip and FWHM as functions of top layer nanoribbon thickness t_1, the distance between two top layer nanoribbons d and top layer nanoribbon width w respectively.

#256039 Received 22 Dec 2015; revised 23 Mar 2016; accepted 18 Apr 2016; published 20 Apr 2016

2.3 Sensing behaviors

The sensing behaviors of the proposed MMDM structure are shown in Fig. 5. When the environmental refractive index (RI) increases from 1.31 to 1.35, a clear red-shift is seen and the resonant wavelength shifts from 1541.1 nm to 1587.8 nm. As shown in Fig. 5(a), both high modulation depth and narrow FWHM keep in the RI range and these are two crucial factors for high sensing performance.The sensitivity S = 1170 nm/RIU from Fig. 5(b). FWHM of the MMDM structure is 1.11 nm, therefore the figure of merit FOM = 1054.

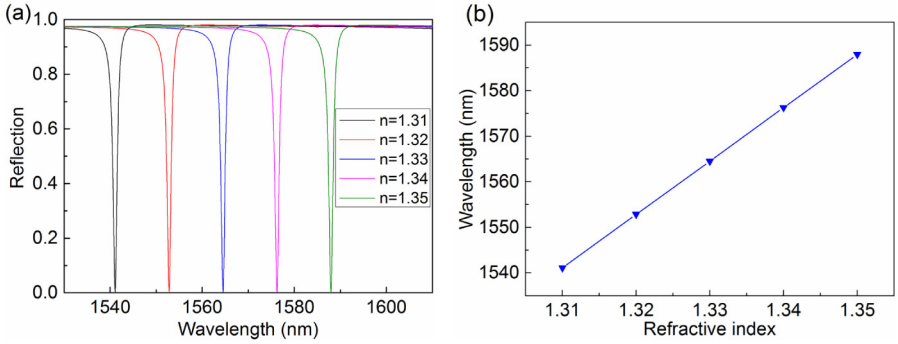

Fig. 5. (a) Reflection spectra of the MMDM structure with various refractive indices of the environment. (b) Resonant wavelength shift against refractive indices. Parameters are set as w = 300 nm, d = 80 nm, t_1 = 60 nm, t_2 = 40 nm, h = 200 nm, P = 1200 nm.

In practical applications, the light intensity change at a fixed wavelength is detected and the corresponding figure of merit can be defined as FOM* = $\max\left|\left(\Delta I/\Delta n\right)/I\right|$, where I is the intensity at the special wavelength and $\Delta I/\Delta n$ is the relative intensity change at a fixed wavelength due to the refractive index change [21]. According to Fig. 6(a), when t_1 changes from 30 nm to 110 nm, FOM increases slightly while FOM* changes strongly. The structure shows good sensing performance for the range of t_1 from 50 nm to 100 nm. Figure 6(b) shows increase of FOM and a maximum of FOM* as d increases. Figure 6(c) also shows increase of FOM and a maximum of FOM* as w increases. These characteristics give us enough guide to design a high performance sensor.

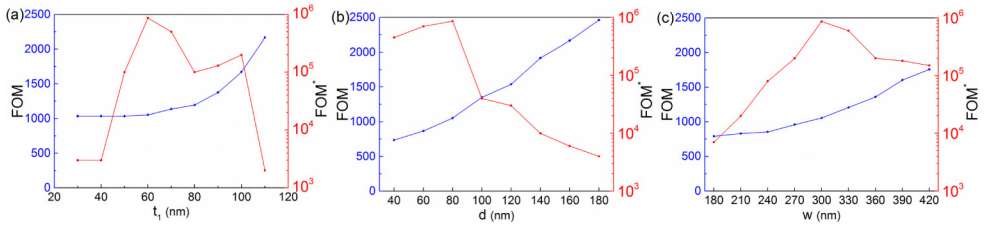

Fig. 6. (a)-(c) FOM and FOM* as functions of top layer nanoribbon thickness t_1, the distance between two top layer nanoribbons d and top layer nanoribbon width w respectively.

3. Conclusion

In summary, we have numerically investigated a perfect narrow band absorber based on the MMDM structure. We obtain a nearly perfect absorption of over 99.9% with an ultra narrow band of 1.11 nm. The absorber can work over a wide range of incident angle with a high absorption. In addition, the structure shows good sensing performance with S of 1170 nm/RIU and FOM of 1054 which has great potential as a biosensor.

#256039 Received 22 Dec 2015; revised 23 Mar 2016; accepted 18 Apr 2016; published 20 Apr 2016

Acknowledgments

This work is supported by the National Projects of Key Scientific Instruments No. 2012YQ16000702 in China.

#256039 Received 22 Dec 2015; revised 23 Mar 2016; accepted 18 Apr 2016; published 20 Apr 2016